Available online at www.sciencedirect.com
ScienceDirect
Journal of Catalysis 251 (2007) 388–399
JOURNAL OF CATALYSIS
www.elsevier.com/locate/jcat

New heterogeneous catalysts for greener routes in the synthesis of fine chemicals

Simona M. Coman [a,*], Georgeta Pop [a], Cristina Stere [a], Vasile I. Parvulescu [a], Jamal El Haskouri [b], Daniel Beltrán [b], Pedro Amorós [b]

[a] *Department of Chemical Technology and Catalysis, Faculty of Chemistry, University of Bucharest, Bdul Regina Elisabeta, 4-12, Bucharest 030016, Romania*
[b] *Institut de Ciencia dels Material, Universitat de Valencia, Valencia E46071, Spain*

Received 2 May 2007; revised 30 July 2007; accepted 1 August 2007

Available online 14 September 2007

Abstract

New strong Lewis acid SnTf-MCM-41 and SnTf-UVM-7 catalysts with unimodal and bimodal pore systems were prepared in a two-step synthesis in which the triflic acid (Tf) was incorporated to previously synthesized mesoporous tin-containing silicas. The Sn incorporation inside the pore walls was carried out through the Atrane method. The SnTf-UVM-7 catalysts were prepared by aggregating nanometric mesoporous particles defining a hierarchic textural-type additional pore system. Following these procedures, catalysts with different Si/Sn ratios—21.8 to 50.8 for SnTf-MCM-41 and 18.4 for SnTf-UVM-7—were prepared. These new materials were tested in the acylation of aromatic sulfonamides using acetic acid as the acylating agent and in the synthesis of (*dl*)-[α]-tocopherol through the condensation of 2,3,6-trimethylhydroquinone (TMHQ) with isophytol (IP). The activity data indicate that these heterogeneous catalysts are very active, corresponding to high yields in acylated compounds as 65.5% and very high selectivity to (*dl*)-[α]-tocopherol (94%, for a conversion of 98%).

Keywords: Heterogeneous catalysis; Mesoporous structures; Tin triflate; Acylated sulfonamides; (*dl*)-[α]-Tocopherol

1. Introduction

Today, there are significant demands by the pharmaceutical industry for new and efficient catalysts. Moreover, together with traditional criteria, such as good activity and selectivity, these new catalysts must include additional requisites, such as low cost and environmental friendliness. Whereas the cost of the process (including catalysts) is not a determinant constraint for specific high-added-value drugs, produced at low scale, it constitutes a first-order parameter when considering generic drugs for diseases affecting a broad population sector or a parapharmaceutical product, such as food complement and/or ingredient or a cosmetic, due to the high production costs involved.

Some newly developed drugs, including therapeutic agents for Alzheimer's disease [1], inhibitors of tRNA synthetases as antibacterial agents [2], and prostaglandin $F_{1\alpha}$ sulfonamides for the potential treatment of osteoporosis, incorporate the *N*-acyl sulfonamide moiety [3]. *N*-acyl sulfonamide synthesis usually starts with the coupling of the parent sulfonamides with acid chlorides or carboxylic anhydrides using trialkylamines, pyridine [2–5], or alkali hydroxides [6–8]. Unfortunately, with no exception, all of these methods lead to substantial waste products; for example, acid chlorides generate hydrochloric acid as byproduct, whereas the carboxylic anhydrides use only 50% of the molecule, achieving low atom economy. Less common reports mentioning this transformation under acidic conditions (Brönsted or Lewis acids) have not systematically examining the purpose and limitations of the reaction [9].

The use of carboxylic acids as acylating agents on alcohol or aromatics is rare [10–15] and usually associated with the presence of hypernucleophilic species (DCC, EDC, or 4-DMAP) (see Aldrich Chemical Company Technical Bulletin AL114). Otherwise, in the case of sulfonamide acylation, besides the above-described synthesis methodologies, routes using carbox-

* Corresponding author.
E-mail addresses: s.coman@chem.unibuc.ro, simona_cmn@yahoo.com (S.M. Coman).

0021-9517/$ – see front matter
doi:10.1016/j.jcat.2007.08.001

ylic acids as a source of carbocation in direct-coupling homogeneous and heterogeneous catalytic processes have been described [16–19]. These latter approximations, which have in common the presence of nucleophilic activators, overcome the undesirable wastes (because water is the main byproduct), and the entire carboxylate amount is reactive.

On the other hand, the synthesis of (*dl*)-[α]-tocopherol is of great importance for the pharmaceutical industry and also in the area of functional foods. In classical synthesis, this is done through the acid-catalyzed condensation of 2,3,6-trimethylhydroquinone (TMHQ) with isophytol (IP) using both Brønsted and Lewis acid catalysts. Corrosion caused by the acidic media, contamination of the wastewater with acids and zinc ions, and the difficult purification of (*dl*)-[α]-tocopherol by distillation under high vacuum at 200 °C are the main problems hindering industrial-scale synthesis [20]. Recently, data concerning the use of heterogeneous catalysts, the main merits of which are the simple separation of the solid catalyst from the reaction mass, the absence of washwater containing the dead catalyst, and a high purity of α-tocopherol, were published [21–23]. Unfortunately, high reaction temperatures and long reaction times are required, leading in many cases to diminished yields as a result of byproduct formation. Recently, some metal derivatives of triflic acid have been suggested as a cleaner alternative to using metal chlorides as Lewis acid and versatile catalysts in organic synthesis [24–26], avoiding such environmental problems as large amounts of waste mineral acids and zinc or aluminum residues, as well as the use of harmful organic solvents in industrial-scale processes.

Keeping this background in mind, and with the aim of designing a greener approach to the above set of reactions, we have prepared new surfactant-assisted mesoporous heterogeneous Sn triflate–silica catalysts. These new family of catalysts combine the high hydrophilic surface and accessible pore system typical of mesoporous silicas with the presence of well-dispersed and anchored tin triflate species able to act as strong acid Lewis catalytic sites. The system architecture has been built up, taking into account the described activity of metal triflate complexes and the compatibility of Sn(IV) and Si(IV) centers in silica networks. Thus we anticipate that our materials will combine the strong Lewis acidity of anchored tin triflate with the water-sink capability of the hydrophilic silica network, becoming efficient coupling-dehydrating agents or active Friedel–Crafts solid catalysts.

Here we report that these new materials are effectively able to facilitate the green acylation of aromatic sulfonamides using acetic acid as an acylating agent. These catalysts are also highly active in the synthesis of (*dl*)-[α]-tocopherol through the condensation of 2,3,6-trimethylhydroquinone (TMHQ) with isophytol (IP).

2. Experimental

2.1. Catalyst preparation

All of the synthesis reagents (tetraethyl orthosilicate [TEOS], triethanolamine [$N(CH_2–CH_2–OH)_3$, hereinafter TEAH3], hexadecyltrimethylammonium bromide [CTABr], $SnCl_2$, triflic acid, NaOH, HCl, and ethanol) were analytically pure and were used as received from Aldrich. The unimodal (SnTf-MCM-41) and bimodal (SnTf-UVM-7) porous catalysts were prepared in a two-step synthesis in which the triflic acid was incorporated into previously synthesized mesoporous tin-containing silicas. The Sn incorporation inside the pore walls was carried out using the Atrane method [27], which enables preparation of a unimodal or bimodal porous mixed oxide working under strong (pH 11 to 12) or moderate (pH 8 to 9) basic conditions, respectively. The resulting tin-doped silicas are designated Sn-MCM-41 and Sn-UVM-7, respectively.

2.1.1. Synthesis of Sn-MCM-41

In a typical synthesis, the molar ratio of the reagents in the mother liquor was adjusted to $2 - x$ Si:x Sn:7 TEAH3:0.5 NaOH:0.52 CTABr:180 H_2O. For example, the Si/Sn = 37 mesoporous material ($x = 0.05$) (working pH = 11) was obtained as follows: 0.5 g (0.0125 mol) of NaOH was dissolved at 60 °C in 23 mL (0.172 mol) of TEAH3, and after a few minutes, 10.7 mL (0.0478 mol) of TEOS and 0.36 g (0.0016 mol) of $SnCl_2$ were added while stirring, and the mixture was heated at 130 °C for 5 min. The resulting solution was cooled to 110 °C, and 4.68 g (0.0128 mol) of CTABr was added under stirring. Then 80 mL (4.44 mol) of water was added under vigorous stirring at a mixing temperature of 60 °C; shortly, a white suspension appeared. This mixture was aged at room temperature for 24 h. The resulting mesostructured powder was filtered off, washed with water and ethanol, and air-dried. Finally, to open the mesopore system, the surfactant was extracted from the as-synthesized solid using an acetic acid/ethanol solution ($CTMA^+/H^+$ exchange). Here ca. 1 g of mesostructured powder was suspended in a solution containing 8 mL of CH_3COOH (80%) and 120 mL of ethanol (99%), and this mixture was heated at reflux (60 °C) for 2 h under stirring. Later, after renewing the CH_3COOH/ethanol solution, and to complete the extraction process, the suspension was reheated at 60 °C for 16 h under stirring. The resulting (mesoporous) powder was collected by filtration, washed with ethanol, and air-dried.

2.1.2. Synthesis of Sn-UVM-7

This mesophase was prepared almost exactly as for Sn-MCM-41, starting from silatrane and stannatrane complexes and working in a TEAH3-rich medium (i.e., using the Atrane route) and in the absence of NaOH (with an apparent working pH of ca. 9.3). Thus the molar ratio of the reagents in the mother liquor was adjusted to $2 - x$ Si:x Sn:7 TEAH3:0.52 CTABr:180 H_2O ($x = 0.1$). In a typical synthesis to obtain the Si/Sn = 26 bimodal porous material, a mixture of TEOS (10.5 mL; 0.047 mol), $SnCl_2$ (0.56 g, 0.0024 mol), and TEAH3 (23 mL, 0.172 mol) was heated at 150 °C for 10 min to prepare Atrane complexes. The resulting solution was cooled to 110 °C, and 4.68 g of CTABr (0.0128 mol) was added. Then 80 mL of water was slowly added under vigorous stirring at 80 °C. After a few minutes, the resulting suspension was aged at room temperature for 4 h. The resulting mesostructured solid was then separated by centrifugation, washed with water and ethanol,

and air-dried. To obtain the final catalyst, the surfactant was chemically extracted as described earlier for Sn-MCM-41. The second step corresponds to the formation of Sn-triflate complexes at the Sn-MCM-41 or the Sn-UVM-7 surface.

2.1.3. Preparation of the SnTf-MCM-41 and SnTf-UVM-7 catalysts

The catalysts were prepared by heating the tin-doped mesoporous silicas in methanolic solutions of triflic acid by the following procedure. A suspension of Sn-MCM-41 or Sn-UVM-7 chemically extracted porous silicas (2 g) was stirred under reflux in a solution of triflic acid (5 g) in methanol (50 mL) for 15 h. The resulting porous samples were collected by filtration, washed with cold methanol to eliminate any excess triflic acid on the silica surface, and air-dried at 80 °C. The obtained samples were designated SnTf-MCM-41 and SnTf-UVM-7.

2.2. Catalyst characterization

All solids were analysed for Sn, Si, and S by electron probe microanalysis (EPMA) using a Philips SEM-515 instrument. X-ray powder diffraction (XRD) data were recorded on a Seifert 3000TT θ–θ diffractometer using CuK_α radiation. Patterns were collected in steps of 0.02° (2θ) over the angular range 1°–10° (2θ) for 25 s per step. To detect the presence of some crystalline bulk phase, additional patterns were recorded with a larger scanning step [0.05° (2θ)] over the angular range 10°–60° (2θ) for 10 s per step. Transmission electron microscopy (TEM) was carried out with a Philips CM-10 electron microscope operating at 100 kV. Samples were ground gently in dodecane, and microparticles were deposited on a holey carbon film supported on a Cu grid. Surface area and pore size values were calculated from nitrogen adsorption–desorption isotherms (−196 °C) recorded on a Micromeritics ASAP-2010 automated instrument. Calcined samples were degassed for 15 h at 130 °C and 10^{-6} Torr before analysis. Surface areas were estimated according to the BET model, and pore size dimensions were calculated using the BJH method. Room-temperature diffuse reflectance spectra were recorded (200–800 nm) using a Shimadzu UV–vis 2501PC spectrophotometer. FTIR spectra were collected on a Nicolet 4700 spectrometer (200 scans with a resolution of 4 cm^{-1}) using self disks of 1% sample in KBr.

2.3. Catalytic tests: Acylation of sulfonamides

In a typical procedure, 1.25 mmol of sulfonamide (benzenesulfonamide, *p*-nitrobenzenesulfonamide, *p*-methoxybenzenesulfonamide) were dissolved in 4 mL of acetonitrile in a 10-mL glass vessel. To this mixture, 3.75 mmol of acylating agent (acetic acid) and 15 mg of catalyst were added (acylating agent:substrate ratio = 3:1). All reactions were carried out at 80 °C for 18 h under vigorous stirring. After the reaction was stopped, the catalyst was filtered off and the product separated from solvent under vacuum at 80 °C as a white crystalline solid. The product was redissolved in the high-pressure liquid chromatography (HPLC) eluent and analyzed under the following conditions: column, GROM-SIL 80 ODS-2 FE; eluent, MeOH, H_2O = 40:60; flow rate, 0.5 mL/min; wavelength, 235 nm; volume sample, 15 μL. The products were characterized by HPLC-MS and ^{1}H NMR techniques.

For comparison, the aforementioned sulfonamides were acylated in the presence of pure $Sn(OTf)_2$ (10 mg). After reaction, 10 mL of saturated aqueous $NaHCO_3$ solution was added, and the products were extracted with Et_2O (20 mL × 2). The organic extract was dried over anhydrous Na_2SO_4 a, after which the solvent was separated from reaction product under vacuum at 80 °C.

For *synthesis of* (*dl*)-[α]-tocopherol, in a typical procedure, 152 mg of TMHQ was dissolved in 10 mL of solvent (acetonitrile, hexane, toluene, DMC, or hexane:DMC [50:50]) in a two-necked flask. Then 50 mg of catalyst was added to this mixture. Once the temperature reached 100 °C, 0.4 mL of IP (TMHQ:IP molar ratio = 1:1) was added dropwise under stirring. The reaction was carried out under reflux conditions for 1 h. After the reaction was stopped, the catalyst was filtered off and the product separated from solvent under vacuum at 80 °C, as light-yellow–brown oil. Yields and purity were determined by HPLC analysis under following conditions: column, EC 125/4.6 NUCLEOSIL 120-5 C18; eluent, acetonitrile; flow rate, 0.8 mL/min; wavelength, 280 nm; volume sample, 15 μL. The compounds were identified with the aid of pure samples (standards).

For comparison, the synthesis of (*dl*)-[α]-tocopherol was done in the presence of pure $Sn(OTf)_2$ (10 mg), using acetonitrile as the solvent. After reaction, saturated aqueous $NaHCO_3$ (10 mL) solution was added and the products were extracted with hexane (20 mL × 2). The organic extract was dried over anhydrous Na_2SO_4, after which the solvent was separated from reaction product under vacuum, at 80 °C, as light-yellow–brown oil.

Recycling tests were carried out as well. After each reaction ended, the catalyst was filtered off, rinsed with the solvent, and dried under ambient conditions for 2 h. Each catalyst was reused in at least four catalytic cycles. Washed catalysts were analyzed by ICP-AES and FTIR.

3. Results and discussion

3.1. Catalyst characterization

As shown in Section 2, the catalysts were prepared in a two-step synthesis in which the triflic acid was incorporated into previously synthesized mesoporous tin-containing silicas. Incorporation of Sn inside the pore walls was done using the Atrane method [27]. The triflate ligands were included following a protocol adapted from the synthesis method described in the bibliography for tin–triflate complexes in solution. The selection of the pH conditions of the first step allowed us to prepare two different catalyst types with a unimodal or bimodal pore system. At high pH values, unimodal Sn-MCM-41, in the form of large micrometric particles, was obtained; working under moderately basic conditions, Sn-UVM-7 materials (a nanometric version of the typical M41 solids) were isolated. These latter catalysts were constructed by aggregating nano-

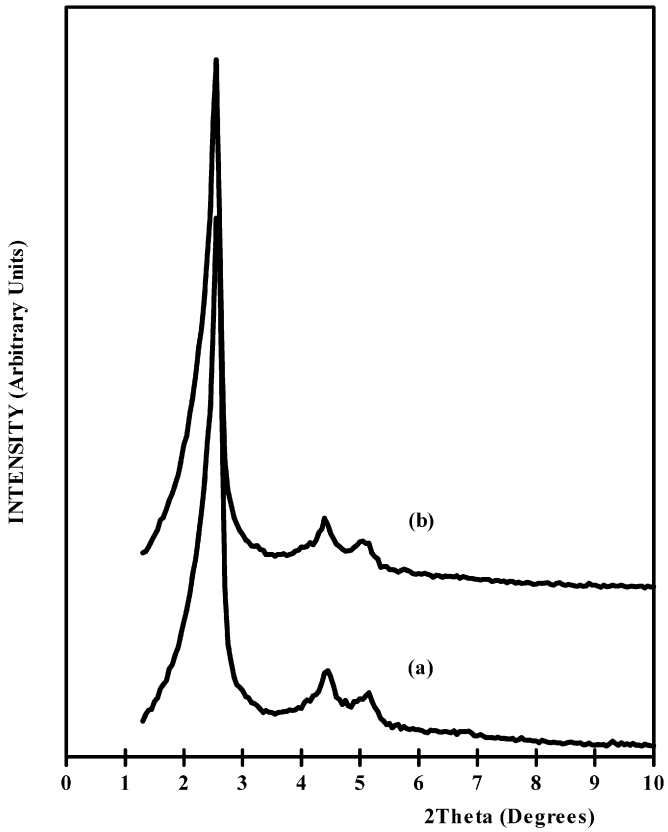

Fig. 1. Low-angle XRD patterns of (a) Sn-MCM-41 and (b) SnTf-MCM-41 catalysts.

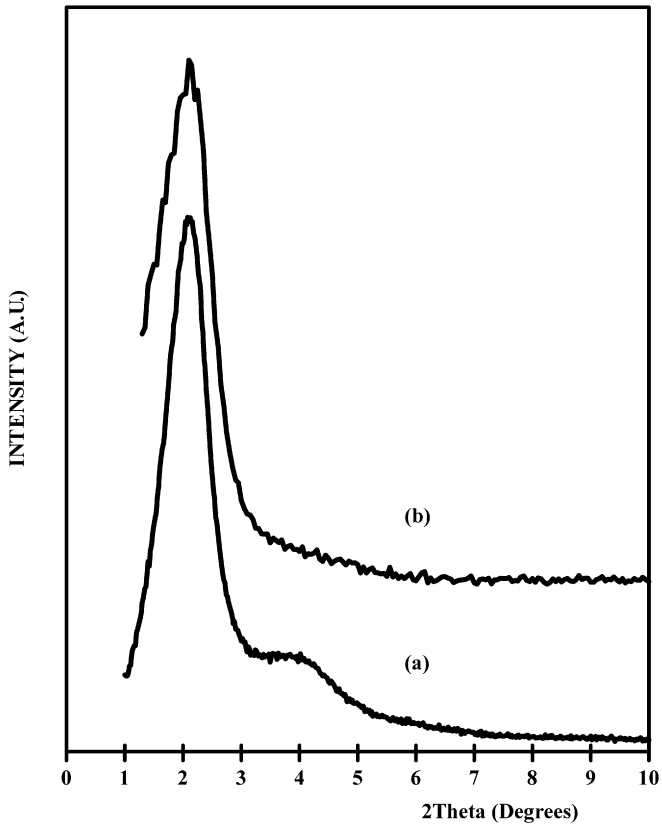

Fig. 2. Low-angle XRD patterns of (a) Sn-UVM-7 and (b) SnTf-UVM-7 catalysts.

metric mesoporous particles defining a hierarchic textural-type additional pore system (UVM-7-like materials). The resulted catalysts are designated SnTf(22)-MCM-41 (Si/Sn = 21.81), SnTf(47)-MCM-41 (Si/Sn = 47.32), SnTf(51)-MCM-41 (Si/Sn = 50.84), and SnTf(18)-UVM-7 (Si/Sn = 18.40).

The symmetry and order degree of the catalysts before and after reaction with triflic acid were studied by XRD and TEM. XRD provides information only on the intraparticle mesopore relative organization (i.e., the surfactant templating pore system). Fig. 1 shows the XRD patterns corresponding to Sn-MCM-41 and SnTf-MCM-41 samples. Both materials display XRD patterns in the low-angle region with one strong diffraction peak, usually associated with the (100) reflection when a hexagonal cell (similar to that described in the case of MCM-41) is assumed, along with two other resolved small signals that can be indexed to the (110) and (200) reflections. These features indicate that the ordered hexagonal mesopore symmetry typical of pure MCM-41 silica was maintained after the Sn incorporation (first step) and even after the reaction with triflic acid (second step).

In a similar way, the disordered intraparticle porosity typical of UVM-7 materials was preserved even after incorporation of Sn as a triflate (Fig. 2). Both solids showed XRD patterns with an intense peak in the low-angle domains, ascribed to the (100) reflection. Apart from the intense peak at low 2θ values, a broad signal of relatively low intensity can be indexed to the overlapped (110) and (200) reflections of the typical hexagonal cell in the case of the Sn-UVM-7 derivative (first step) that practically disappeared after reaction with triflic acid (second step). In both series (MCM-41 and UVM-7 like), the peak positions remained practically unchanged. This finding confirms that the mesostructures were not altered after reaction with triflic acid/methanol and thus supports our selection of solvent. In fact, a significant loss of order (and consequently mesostructure degradation) was observed in preliminary syntheses carried out in acetonitrile as solvent. On the other hand, the second reaction step affected the signal intensities only slightly. The small loss of X-ray intensity observed in the XRD corresponding to SnTf-MCM-41 and SnTf-UVM-7 (compared with Sn-MCM-41 and Sn-UVM-7, respectively) must be attributed to a certain phase-cancellation phenomena associated to the introduction of scattering material (triflate anions) into the pores, although the possibility of a slight decrease in symmetry cannot be discarded. In all samples, the absence of XRD peaks at high angle values indicates that no phase segregation leading to SnO or SnO_2 bulk oxides occurred.

The TEM images (Figs. 3a, 3b) were completely correlated with XRD observations. The observation in both cases of a dominant (single-type) particle morphology supports the monophasic nature of the catalysts. Typical morphologies—hexagonal ordered large particles and aggregates of disordered nanoparticles—were observed for the SnTf-MCM-41 and SnTf-UVM-7 catalysts. Moreover, TEM images of both catalysts also showed small dark spots (average size ca. 2 nm) that could be due to Sn-rich domains.

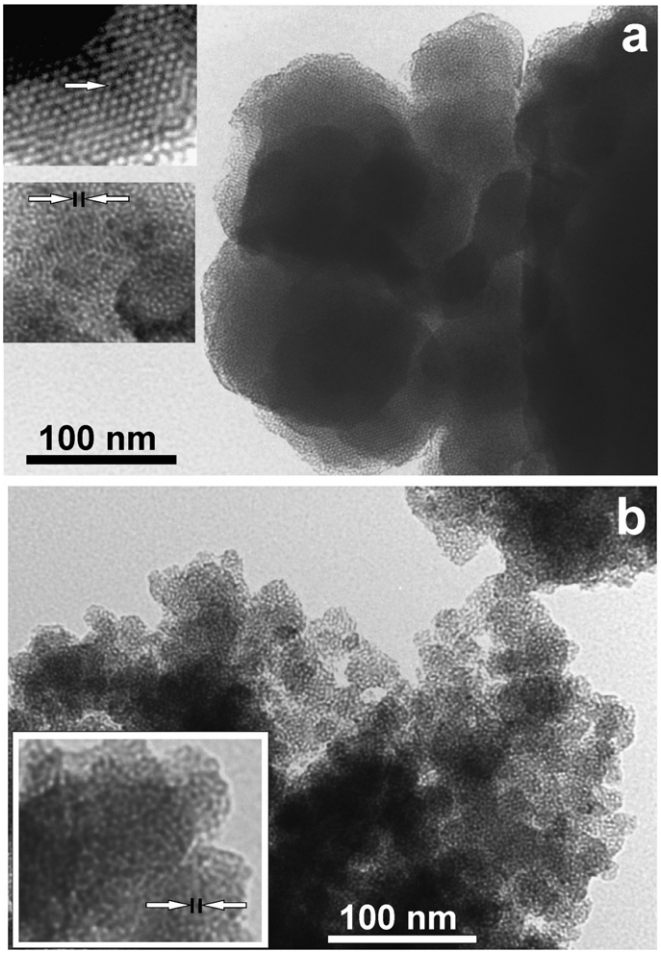

Fig. 3. TEM images of (a) SnTf-MCM-41 [the insets show enlarged TEM images showing the ordered pore array (×5) and the rich Sn domains (×3)] and (b) SnTf-UVM-7 catalysts [the inset shows an enlarged (×3) TEM image].

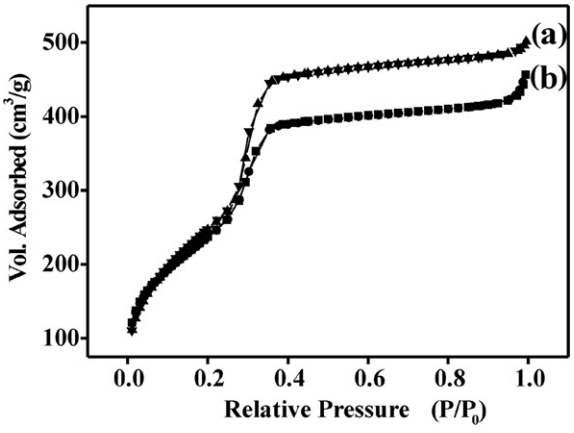

Fig. 4. N_2 adsorption–desorption isotherms of (a) Sn-MCM-41 and (b) SnTf-MCM-41 catalysts.

The unimodal and bimodal porous character of MCM-41 and UVM-7-like catalysts was further confirmed by N_2 adsorption–desorption isotherms (Figs. 4 and 5). All samples presented a clear and sharp adsorption step at intermediate relative pressure values ($0.15 < P/P_0 < 0.4$) due to the capillary condensation of N_2 inside the intra-nanoparticle surfactant-templated mesopores. Moreover, the isotherms of UVM-7-like catalysts showed a second adsorption step at high relative pressure values ($P/P_0 > 0.8$), associated with filling of the large interparticle cage-like pores. In both series, the unimodal or bimodal porous topology together with a high BET surface area was maintained before and after reaction with triflic acid (Table 1). The pore size after this second reaction step was practically unaltered, with only a slight decrease of both parameters observed. This evolution supports the insertion of triflate anions inside the pores.

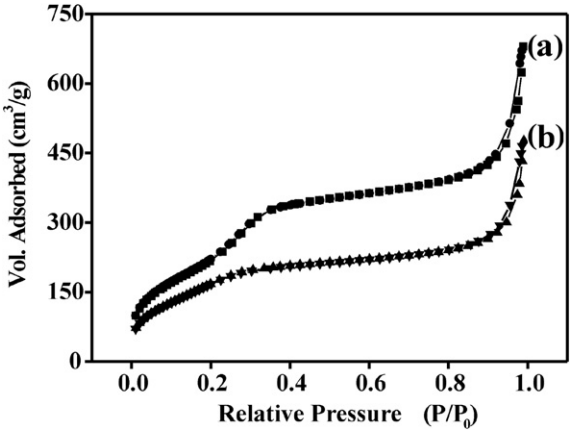

Fig. 5. N_2 adsorption–desorption isotherms of (a) Sn-UVM-7 and (b) SnTf-UVM-7 catalysts.

Fig. 6 shows more evidence on the formation of the Sn triflate species. FTIR spectra indicate that the MCM-41 and UVM-7 supports did not retain even a trace of triflate. In contrast, on doped Sn-silica samples, triflic acid was incorporated in amounts that increased with increasing Sn content. No anchoring occurred on the silica wall, but anchoring was obvious on the Sn sites and on the Sn silica. The results of chemical analysis and TGA of these samples were consistent with FTIR results and with the reported S/Si ratios.

A summary of the textural and chemical characteristics of the prepared catalysts is given in Table 1.

3.2. Catalytic behavior in acylation of various sulfonamides with acetic acid

The aforementioned catalysts were tested in the acylation of benzenesulfonamide (**1a**, R = H), *p*-nitrobenzenesulfonamide (**1b**, R = NO_2), and *p*-methoxybenzenesulfonamide (**1c**, R = MeO) with acetic acid (Scheme 1). The only byproduct in this case was water. Data presented in Table 2 confirm that in the presence of these catalysts, the acylation of the above substrates with acetic acid, which usually requires high temperatures (necessary to activate the acylating agent), occurred with yields from moderate to good even at temperatures as low as 80 °C. Of note, the selectivity was 100% irrespective of the structure of the substrate or the nature of the catalyst. On the other hand, the fact that for Sn-MCM and Sn-UVM, neither triflic acid-impregnated support had any activity in this reaction provides additional evidence that the active site was associated with tin triflate species.

Table 1
The textural and chemical characteristics of the SnTf-MCM-41 and SnTf-UVM-7 samples

	Sample	Si/Sn[a]	Sn/S[a]	d_{100} (nm)[b]	S_{BET} (m^2/g)	Small pore (nm)[c]	Large pore (nm)[c]
1	Sn-MCM-41	38.0	–	4.0	937	2.5	–
2	SnTf(22)-MCM-41	21.8	2.3	4.1	725	2.5	–
3	SnTf(47)-MCM-41	47.3	1.4	3.7	878	2.6	–
4	SnTf(51)-MCM-41	50.8	1.3	3.7	812	3.1	–
5	Sn-UVM-7	19.0	–	4.8	820	2.4	32.3
6	SnTf(18)-UVM-7	18.4	1.1	4.5	646	2.1	36.6

[a] Si/Sn and Sn/S molar ratio estimated from electron probe microanalysis (EPMA).
[b] Cell parameter calculated assuming a hexagonal cell (XRD).
[c] Textural characteristics from the adsorption–desorption isotherms of liquid N_2 at 77 K.

Table 2
The *N*-acyl sulfonamides yield and TOF as a function of the substrate and the catalyst nature

	Catalyst	Substrate	Yield (%)	TOF (h^{-1})
1	SnTf(22)-MCM-41	Benzenesulfonamide	30.0	8.9
2	SnTf(22)-MCM-41	*p*-Nitrobenzenesulfonamide	17.4	2.8
3	SnTf(47)-MCM-41	Benzenesulfonamide	45.2	9.1
4	SnTf(47)-MCM-41	*p*-Nitrobenzenesulfonamide	11.4	2.9
5	SnTf(51)-MCM-41	Benzenesulfonamide	48.6	9.3
6	SnTf(51)-MCM-41	*p*-Nitrobenzenesulfonamide	11.7	2.3
7	SnTf(18)-UVM-7	Benzenesulfonamide	65.5	4.6
8	SnTf(18)-UVM-7	*p*-Nitrobenzenesulfonamide	24.2	1.7
9[a]	$Sn(OTf)_2$	Benzenesulfonamide	76.0	9.9
10[a]	$Sn(OTf)_2$	*p*-Nitrobenzenesulfonamide	26.1	3.4

Note. Conditions: substrate (1.25 mmol), acetic acid (3.75 mmol), catalyst: (15 mg), solvent (4 mL of acetonitrile), reaction temperature (80 °C), reaction time (18 h).
[a] Catalyst: (10 mg), reaction time (4 h).

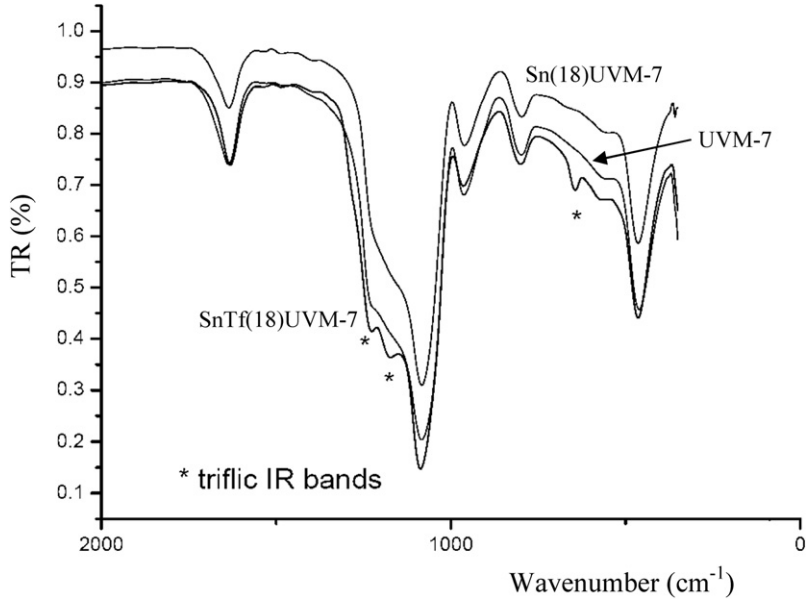

Fig. 6. Comparative FTIR spectra of UVM-7, Sn(18)-UVM-7 and SnTf(18)-UVM-7 samples.

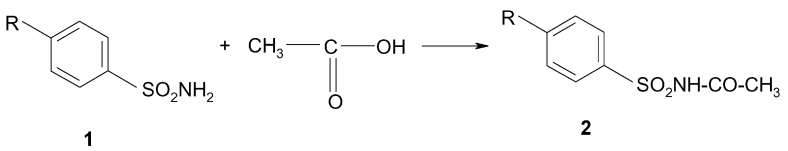

1a: R=H; **1b**: R=NO2; **1c**: R=MeO

Scheme 1. The acylation of aromatic sulfonamides.

The nucleophilic substrates reaction rate with acylium cations would be expected to increase as the induced electronic density on C4 and thus the N basicity increase. Nevertheless, the observed rate of the sulfonamide acylation followed the sequence benzenesulfonamide > *p*-nitrobenzenesulfonamide > *p*-methoxybenzenesulfonamide and was very sensitive to the nature of the aromatic hydrogen substituent. The selectivity in acylated *p*-methoxybenzenesulfonamide did not exceed 7% irrespective of the catalyst nature. This corresponds to an approximate relative yield of benzenesulfonamide: *p*-nitrobenzenesulfonamide: *p*-methoxybenzenesulfonamide of 10:4:1 (Table 2). This result contrasts with that obtained from Brönsted acid (i.e., sulfuric)-catalyzed homogeneous acylation of the same substrate set using acetic anhydride in the same solvent and conditions, where yield (98%, 95%, 91% for R = NO_2, H, OMe, respectively) did not significantly depend on the nucleophile's substituent nature [18]. The catalysts nature is obviously responsible for the behavior observed in our system.

The best yield (65.5%; entry 7, Table 2) to acylated sulfonamides **2** was obtained in the presence of the SnTf(18)-UVM-7 catalyst (Si/Sn ratio = 18.40). In heterogeneous acidic catalysis, isolated species usually are much more active than oligomeric and polymeric species. In conventional co-hydrolysis methods, good dispersion of monomeric Sn in the silica network is not easily achieved. The hydrolysis rate of tin (IV) is much higher than that of silicium, with subsequent low chemical homogeneity and even phase segregation. Therefore, the Atrane route to Sn-MCM-41 synthesis provides an attractive solution, favoring the harmonic heterometallic hydrolysis–condensation processes. With this preparation method, high concentrations of well-dispersed Sn atoms into the framework of the mesoporous silica can be attained. Regardless of the support type (MCM-41 or UVM-7), UV–vis characterization suggested the presence of highly dispersed tetrahedral isolated Sn^{4+} with an absorption band centered at 250 nm, ascribed to charge transition from O^{2-} to Sn^{4+} in a tetrahedral coordination environment [28]. In the SnTf(18)-UVM-7 sample, these Sn sites seemed to be the dominant Sn^{4+} species. However, in the SnTf-MCM-41 catalysts, the additional observed band (centered at ca. 289 nm, assigned to charge transitions from O^{2-} to Sn^{4+} in octahedral environments with a certain degree of polymerization [29]) could be associated with the existence of small casiterite-like nanodomains (Fig. 7) with a subsequent decrease in active sites from ca. 30 to 50% for low and high Sn-containing MCM-41 samples, respectively. This tendency to form Sn–O–Sn bonds is due to the higher pH values used for preparing MCM-41 materials compared with that used for preparing UVM-7. Moreover, chemical analysis of the reaction products clearly indicated no leaching of the active species. The presence of Sn^{4+} sites was also suggested by XPS measurements. The values measured for the Sn 3d5/2 species were closer to those of Sn^{4+} than those of Sn^{2+} [30,31].

Scheme 2 proposes a model of the active sites in the investigated catalysts. TOF values given in Table 2 and their correlation with the molar concentration of the highly dispersed tin triflate ($Sn(OTf)_x$) are in line with this model. Fig. 8 shows the variation of TOF with the content of $Sn(OTf)_x$ species and

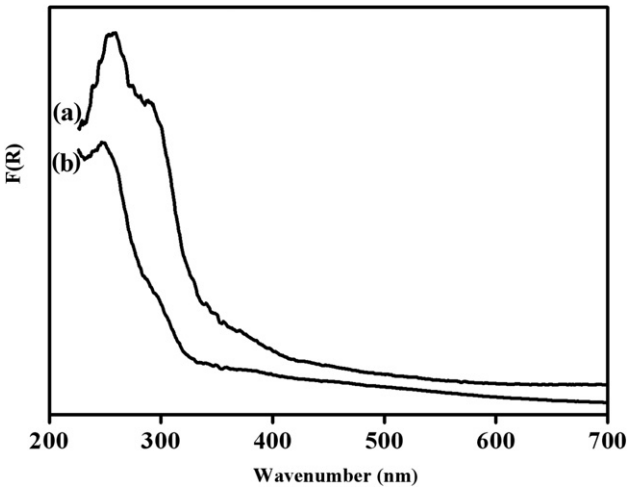

Fig. 7. Diffuse reflectance UV–vis spectra of (a) SnTf-MCM-41 and (b) SnTf-UVM-7 catalysts.

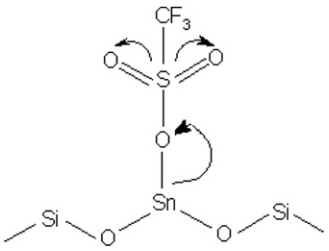

Scheme 2. The model of the active site in incorporated Sn-triflate catalysts.

the Si/Sn ratio. The increased concentration of the $Sn_y(O,OH)_z$ species exhibited a negative effect on the yield. These data also demonstrated that the network in which Sn is incorporated is very important, making it more or less accessible to complexation by triflate. Although the concentration of Sn increased from SnTf(51) to SnTf(22), neither the evolution of TOF nor the concentration of $Sn(OTf)_x$ followed the same trend, demonstrating the contribution of isolated $Sn(OTf)_x$ sites in this reaction.

The additional experiments carried out in homogeneous conditions using pure $Sn(OTf)_2$ (entries 9 and 10, Table 2) confirmed the foregoing conclusion about the contribution of the isolated $Sn(OTf)_x$ sites. The TOFs measured for this catalyst were slightly higher than those found for heterogeneous catalysts; however, the differences were enough small to indicate that the homogeneous system is more active.

The observed tendency toward formation of Sn–O–Sn bonds and the small amount of triflate ligands in the SnTf(22)-MCM-41 dropped the proportion of active $Sn(OTf)_x$ sites compared with SnTf(51)-MCM-41, in accordance with the catalytic results. Thus, the pH value at the first reaction step can be considered the key to controlling the concentration of active sites, avoiding basic high-coordinated $Sn_y(O,OH)_z$ species or SnO_2 segregation. Under moderate basic conditions, the cross-condensation among Si and Sn species is favored, and SnTf-UVM-7 catalysts must have significantly higher amounts of active sites than SnTf(22)-MCM-41 with similar Si/Sn ratios. Moreover, the low Sn/S = 1.1 molar ratio in UVM-7 catalysts warrants that all tin surface sites exist as tin-triflate centers (Ta-

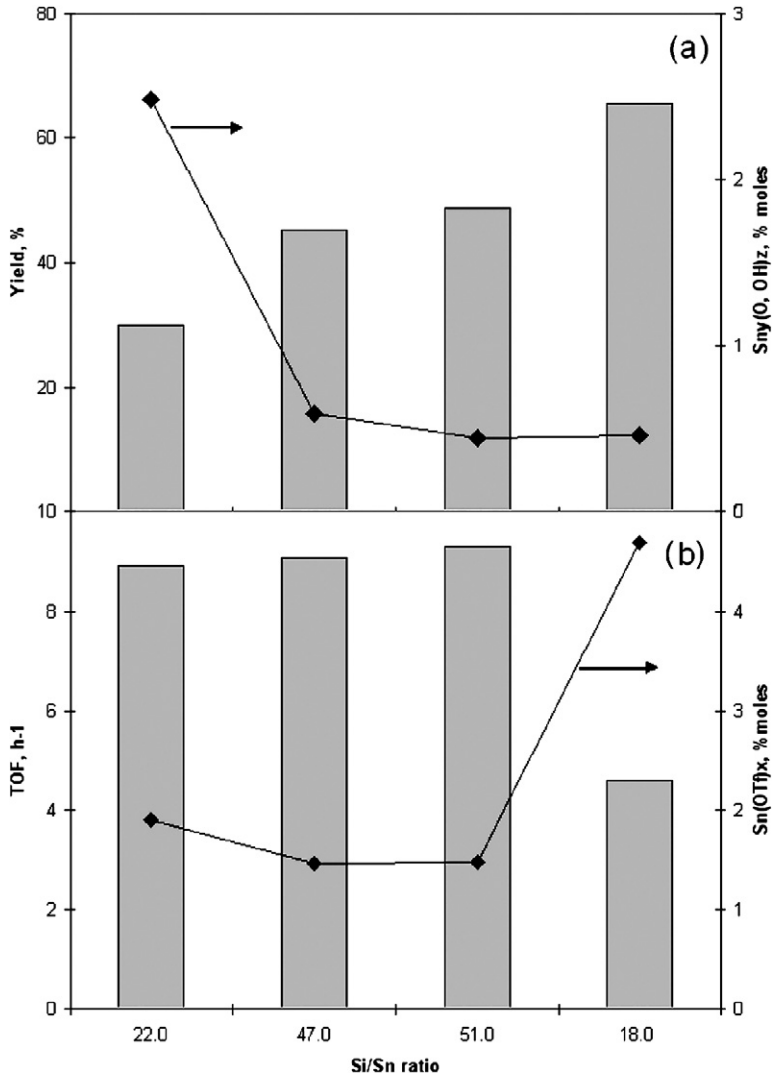

Fig. 8. The variation of the yield to acyl-benzenesulfonamide (a) and TOF (b) with the content of $Sn(OTf)_x$ species and Si/Sn ratio in the acylation of benzenesulfonamide with acetic acid (Si/Sn = 22.0, 47.0 and 51.0 for MCM structure, Si/Sn = 18.0 for UVM structure).

ble 1) with a Sn/triflate proportion of between 1 and 2. The superacid active site of the catalyst would be the anchored $Sn(OTf)_x$ species, and the silica network would be the dehydrating agent. Recycling experiments revealed no deactivation in this reaction.

3.3. Catalytic behavior in the condensation of the 2,3,6-trimethylhydroquinone with isophytol

To extend the scope of application of these catalysts, the condensation of the 2,3,6-trimethylhydroquinone (TMHQ, **3**) with isophytol (IP, **4**) for the synthesis of (*dl*)-[α]-tocopherol (**5**) was attempted (Scheme 3). This synthesis occurs in two steps: (i) chemoselective acid-catalyzed Friedel–Crafts alkylation of trimethylhydroquinone (TMHQ) with isophytol, and (ii) chromane ring closure. The nature of the solvent is very important for this reaction (Table 3). The best solvent seems to be a nonpolar solvent (e.g., hexane, $\varepsilon = 2.02$). As the polarity of the solvent increased, the catalytic performances became poorer; thus in acetonitrile ($\varepsilon = 36.6$), the conversion of TMHQ was ca. 60%. This can possibly explained by the carbocation stabilization in polar solvents by strong ion dipole interactions.

We observe that every tested material exhibited excellent conversion rates regardless of the Si/Sn or Sn/S ratio. Nevertheless, when referring to reaction selectivity, the behavior differed; as it occurred in the case of sulfonamide acylation, well-dispersed $Sn(OTf)_x$ species seemed to affect the catalytic performance. The selectivity to (*dl*)-[α]-tocopherol was high for catalysts with a low oligomeric tin species content (Fig. 9a). Thus, optimum results were obtained for SnTf(51)-MCM-41, whereas SnTf(22)-MCM-41 exhibited very poor selectivity. (In fact, this latter material would be considered a selective catalyst for the benzofurane derivative.) Again, SnTf(18)-UVM-7 was more selective to (*dl*)-[α]-tocopherol than SnTf(22)-MCM-41 irrespective of the nature of the solvent and demonstrated similar (but somewhat poorer) performance than SnTf(51)-MCM-41 (see Table 4). The tin-triflated UVM-7 silicas were not optimized; SnTf(18)-UVM-7 gave reasonable results, but a lower Si/Sn ratio would be expected to give this material better selectivity in tocopherol synthesis.

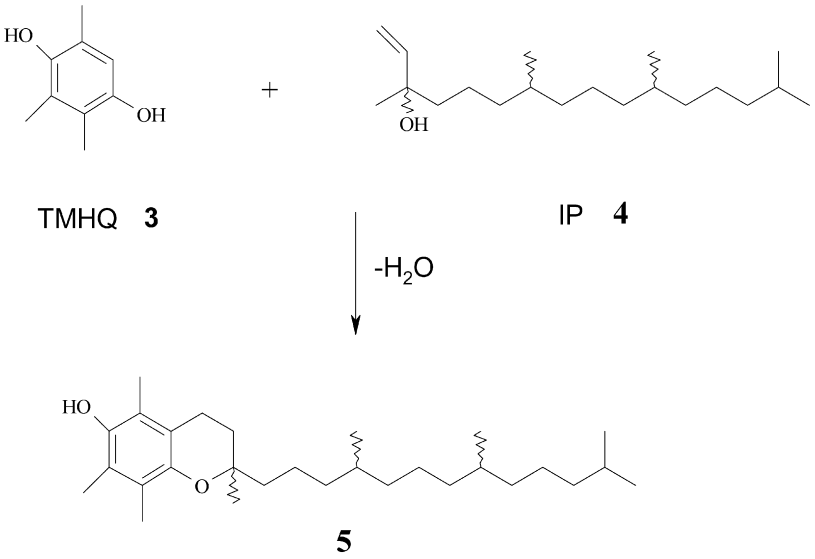

Scheme 3. The synthesis of (*dl*)-[α]-tocopherol **5** by the condensation of TMHQ **3** and IP **4**.

Table 3
The TMHQ conversion, TOF and (*dl*)-[α]-tocopherol selectivity as a function of the solvent nature

Catalyst/ solvent	SnTf(22)-MCM-41			SnTf(18)-UVM-7		
	Conversion (%)	TOF (h^{-1})	Selectivity (%)	Conversion (%)	TOF (h^{-1})	Selectivity (%)
Hexane	99.8	69.8	13.0	100	30.6	76.5
Toluene	93.1	65.1	19.2	97.3	29.8	46.7
DMC	90.3	63.1	15.0	92.7	28.3	20.5
Acetonitrile	58.5	40.9	10.3	61.8	18.9	67.9

Note. Conditions: TMHQ (152 mg), IP (0.4 mL), solvent (10 mL), catalyst (50 mg), reaction temperature (100 °C), time (1 h); Conversion and selectivity are based on TMHQ by HPLC-analysis of isolated material.

Fig. 9 shows the way in which the selectivity (Fig. 9a) and TOF (Fig. 9b) correlate with the content of $Sn_y(O,OH)_z$ and $Sn(OTf)_x$ species and the Si/Sn ratio. As for the acylation of sulfonamides for MCM-41-type catalysts, even though the Sn concentration increased from SnTf(51) to SnTf(22), neither the evolution of TOF nor the concentration of $Sn(OTf)_x$ followed the same trend, thus demonstrating the effect of highly dispersed $Sn(OTf)_x$ sites in this reaction. On the other hand, Fig. 9a shows a negative effect of low-coordinated $Sn_y(O,OH)_z$ species in this reaction. As expected, the increased concentration of these species caused a decrease in the selectivity to (*dl*)-[α]-tocopherol.

Table 4 also presents data collected for the $Sn(OTf)_2$ catalyst (entry 5). As for the acylation of sulfonamides, TOF was in the same range as that of the most active MCM-41-type catalysts, providing another argument for the activity of dispersed tin-triflate species. The selectivity to (*dl*)-[α]-tocopherol serves as more evidence in this sense.

The mechanistic details of the alkylation step involves the interaction of an alkylating agent (isophytol) with the protons generated through the interaction of the acid catalyst with the solvent to form an activated electrophile, which adds to the aromatic ring of TMHQ acting as a nucleophile, followed by proton elimination. The availability and proportion of the different carbocations (*i*-phytil, *n*-phytil, and all isomeric phytadienes) [32] seems to be the key step in successful synthesis. Specially, the benzofuran derivative/(*dl*)-[α]-tocopherol ratio is a function of the relative stability of *i*-phytil and *n*-phytil cations. It is very well known that the stability of the carbenium ions follows the sequence primary < secondary < tertiary, whereas their reactivity follows the sequence primary > secondary > tertiary. As a result, the benzofurane derivative is the principal byproduct due to *i*-phytil–*n*-phytil cation isomerization. Moreover, phytadienes readily undergo polymerization and condense with TMHQ to form mixtures of "isomeric" tocopherols that are heterocyclic in nature. Then the benzofurane derivatives are not the only byproduct in this reaction. It is well known that alcohols, preferably tertiary allylic alcohols like **4**, readily dehydrate in the presence of acids [33]. Others have reported that formation of some other intermediates and byproducts is also possible [34,35]. The solvent itself also can be a source of byproducts.

The ground-state activated electrophile (isophyl species) forms relatively tight ion pairs with the $Sn(OTf)_x$ species and may show a considerable degree of covalent bonding. However, basic $Sn_y(O,OH)_z$ oligomers present on the silica surface will compete with monomers as carbocation-bonding centers. The *i*-phytil and *n*-phytil cations, which have different charges (and acidities), interact with all tin centers on the surface. The strongest interaction, between *n*-phytil and basic $Sn_y(O,OH)_z$

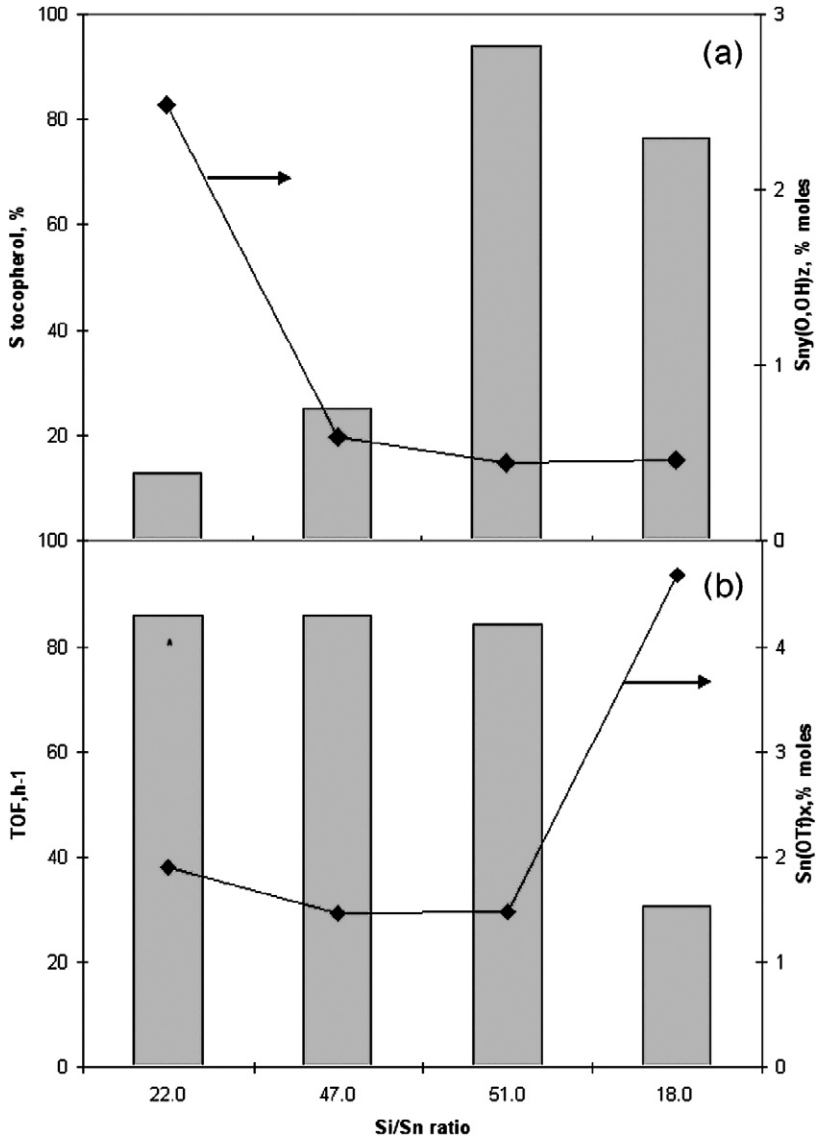

Fig. 9. The variation of the selectivity to tocopherol (a) and TOF (b) with the content of $Sn(OTf)_x$ species and Si/Sn ratio in the synthesis of tocopherol (Si/Sn = 22.0, 47.0 and 51.0 for MCM structure, Si/Sn = 18.0 for UVM structure); after 50 min.

Table 4
The TMHQ conversion, TOF and (*dl*)-[α]-tocopherol selectivity as a function of the Si/Sn ratio

	Sample	Si/Sn[a]	Sn/S[a]	Conversion (%)[b]	TOF (h^{-1})	Selectivity (%)[b]
1	SnTf(22)-MCM-41	21.8	2.3	99.8	69.8	13.0
2	SnTf(47)-MCM-41	47.3	1.4	99.0	86.1	25.2
3	SnTf(51)-MCM-41	50.8	1.3	98.0	84.5	94.0
4	SnTf(18)-UVM-7	18.0	1.1	100	30.6	76.5
5[c]	$Sn(OTf)_2$	–	–	100	83.4	95.2

[a] Si/Sn and Sn/S molar ratio estimated from electron probe microanalysis (EPMA).
[b] Conditions: TMHQ (152 mg), IP (0.4 mL), solvent (hexane, 10 mL), catalyst (50 mg), reaction temperature (100 °C), time (1 h).
[c] Solvent (acetonitrile, 10 mL), catalyst (10 mg), reaction time (30 min). Conversion and selectivity are based on TMHQ by HPLC-analysis of isolated material.

domains, will prevent the desired TMHQ alkylation. The tin-rich catalysts (obtained at high pH values) will give the poorest results.

Table 5 presents the results of recycling the SnTf(51)-MCM-41 catalysts in the synthesis of (*dl*)-[α]-tocopherol. After four cycles, the conversion of TMHQ was preserved at >80%. In addition, the decrease in selectivity to (*dl*)-[α]-tocopherol was <10% after four cycles. These data demonstrate that the investigated catalysts are quite robust in a reaction for which previous reports claimed rapid catalyst deactivation [36,37].

Fig. 10 shows typical FTIR spectra collected for the SnTf(51)-MCM catalyst tested in this reaction after its separation

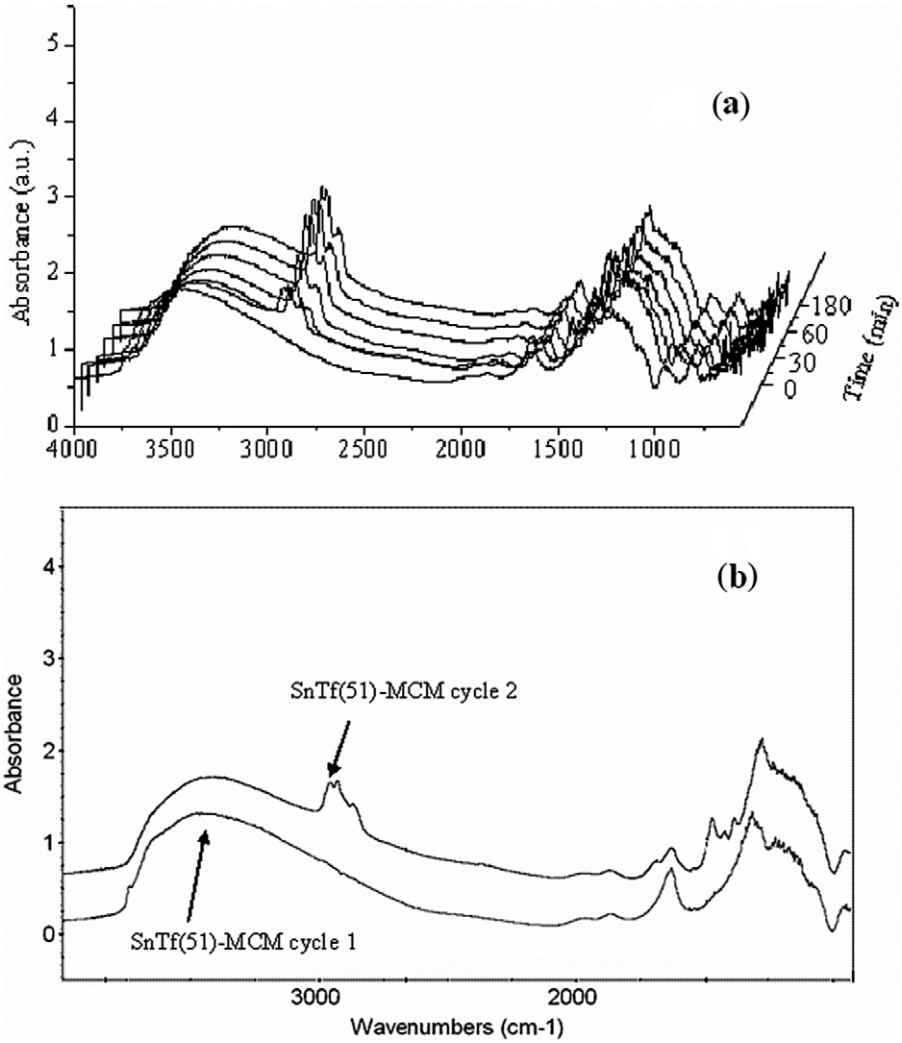

Fig. 10. The FTIR spectra collected for the SnTf(51)-MCM-41 sample (a) in time and (b) after the first recycling.

Table 5
Synthesis of (*dl*)-[α]-tocopherol with reused, non-regenerated SnTf(51)-MCM-41 catalyst

Catalytic cycle	Conversion (%)	Selectivity (%)	TOF (h^{-1})
1 (fresh catalyst)	98.0	94.0	84.5
2	90.0	93.6	77.6
3	81.4	90.1	70.2
4	80.0	86.0	70.0

Note. Conditions: TMHQ (152 mg), IP (0.4 mL), solvent (hexane, 10 mL), catalyst (50 mg), reaction temperature (100 °C), time (1 h); conversion and selectivity are based on TMHQ by HPLC-analysis of isolated material.

at different reaction times. Initially, the spectrum of the fresh catalyst showed only bands assigned to support and triflate species; however, after 30 min, new bands at 2900–2800 cm^{-1}, assigned to $–OCH_2$ and $–CH_2$ groups, were detected. The intensity of these bands reached a plateau after 1 h of reaction. These bands were assigned to strongly chemisorbed IP and byproduct molecules on the most active triflate species. Thus, the decreased catalyst activity is likely related to blockage of the very active sites by these compounds. To confirm this supposition, the catalyst recovered after 1 h of reaction was rinsed with the solvent and recycled; the results were very similar to those presented in Table 5 for the second recycle. In this way, we also can also explain the decrease of the TOF in the second cycle and the slight decrease of the selectivity (Table 5). Spectra presented in Fig. 10b confirm this behavior.

Therefore, this new catalyst family is characterized by a triple functionality: (i) the Lewis $Sn(OTf)_x$ activating centers, which generate carbocations; (ii) the basic blocking $Sn_y(O,OH)_z$ oligomers, which account for the yield variations observed in the sulfonamide acylation and, with respect to the Friedel–Crafts alkylation, are able to modulate the isophyl equilibrium affecting then the selectivity; and (iii) the high-surface area silica as the necessary dehydrating support. This latter aspect is most important, because keeping water away allows working at temperatures below the boiling point of water.

4. Conclusion

Our data demonstrate that in the investigated SnTf-MCM-41 and SnTf-UVM-7 catalysts, triflate is associated with well-dispersed tin species. The synthesis of these catalysts was achieved in two steps, with triflic acid incorporated into previ-

ously synthesized mesoporous tin-containing silicas for Sn content up to Si/Sn > 18. Both SnTf-MCM-41 and SnTf-UVM-7 are highly active green catalysts for acylation with acetic acid and synthesis of (*dl*)-[α]-tocopherol.

Acknowledgments

The authors thank the MEC (projects MAT2003-08568-C03-01 and CTQ2006-15456-C04-03) for support. J.E.H. also thanks the MEC for a Ramón & Cajal contract.

References

[1] T. Hasegawa, H. Yamamoto, Bull. Chem. Soc. Jpn. 73 (2000) 423.
[2] M.G. Banwell, C.F. Crasto, C.J. Easton, A.K. Forrest, T. Karoli, D.R. March, L. Mensah, M.R. Nairn, P.J. O'Hanlon, M.D. Oldham, W. Yue, Bioorg. Med. Chem. Lett. 10 (2000) 2263.
[3] Y. Wang, D.L. Soper, M.J. Dirr, M.A. DeLong, B. De, J.A. Wos, Chem. Pharm. Bull. 48 (2000) 1332.
[4] K. Kondo, E. Sekimoto, J. Nakao, Y. Murakami, Tetrahedron 56 (2000) 5843.
[5] K. Kondo, E. Sekimoto, K. Miki, Y. Murakami, J. Chem. Soc. Perkin Trans. 1 (1998) 2973.
[6] N. Ishizuka, K.-I. Matsumura, K. Hayashi, K. Sakai, T. Yamamori, Synthesis 6 (2000) 784.
[7] N. Ishizuka, K. Matsumura, Japanese Patent JP-10045705, 1998.
[8] T. Inoe, O. Myahara, A. Takahashi, Y. Nakamura, Japanese Patent JP-08198840, 1996.
[9] Y. Morisawa, M. Kataoka, H. Negahori, T. Sakamoto, N. Kitano, K. Kusano, J. Med. Chem. 23 (1980) 1376.
[10] M. Akçay, Appl. Catal. A Gen. 269 (2004) 157.
[11] C.L. Padró, C.R. Apesteguía, J. Catal. 226 (2004) 308.
[12] A.K. Pandey, A.P. Singh, Catal. Lett. 44 (1997) 129.
[13] I. Neves, F. Jayat, P. Magnoux, G. Pérot, F.R. Ribeiro, M. Gubelmann, M. Guisnet, J. Mol. Catal. 93 (1994) 169.
[14] V.D. Kumari, G. Saroja, A. Ratnamala, M. Noorjahan, M. Subrahmanyam, React. Kinet. Catal. Lett. 79 (2003) 43.
[15] J.M. Escola, M.E. Davis, Appl. Catal. A Gen. 214 (2001) 111.
[16] P. Gomes, J.R.B. Gomes, M. Rodrigues, R. Moreira, Tetrahedron 59 (2003) 7473.
[17] A.R. Katrizky, S. Hoffmann, K. Suzuki, ARKIVOC 12 (2004) 14.
[18] M.T. Martin, F. Roschangar, F.F. Eaddy, Tetrahedron Lett. 44 (2003) 5461.
[19] I.E. Pop, B.P. Déprez, A.L. Tartar, J. Org. Chem. 62 (1997) 2594.
[20] T. Netscher, Chimica 50 (1996) 563.
[21] F. Schager, W. Bonrath, J. Catal. 1 (1999) 282.
[22] R.F. Childs, A. Mika-Gibala, J. Org. Chem. 47 (1982) 4207.
[23] A. Heidekum, M.A. Harmer, W.F. Hölderich, J. Catal. 176 (1998) 260.
[24] S. Luo, L. Zhu, A. Talukdar, G. Zhang, X. Mi, J.-P. Cheng, P.G. Wang, Mini Rev. Org. Chem. 2 (2005) 546.
[25] S. Kobayashi, M. Sugira, H. Kitagawa, W.W.-L. Lam, Chem. Rev. 102 (2002) 2227.
[26] A. Corma, H. Garcia, Chem. Rev. 103 (2003) 4307.
[27] S. Cabrera, J. El Haskouri, C. Guillem, J. Latorre, A. Beltrán, D. Beltrán, M.D. Marcos, P. Amorós, Solid State Sci. 2 (2000) 405.
[28] S. Samanta, N.K. Mal, A. Manna, A. Bhaumik, Appl. Catal. A Gen. 273 (2004) 157.
[29] Z.C. Liu, H.R. Chen, W.M. Huang, J.L. Gu, W.B. Bu, Z.L. Hua, J.L. Shi, Microporous Mesoporous Mater. 89 (2006) 270.
[30] C.D. Wagner, J.F. Moulder, L.E. Davis, W.M. Riggs, Handbook of X-Ray Photoelectron Spectroscopy, Perking–Elmer Corporation, Physical Electronics Division, 1993.
[31] D. Briggs, M.P. Seah, Practical Surface Analysis, vol. 1, Auger and X-Ray Photoelectron Spectroscopy, second ed., Wiley/Salle & Sauerländer, Chichester, New York, Brisbane, Toronto, Singapore/Aarau, Frankfurt/M, Salzburg, 1990.
[32] J. March, Advanced Organic Chemistry, third ed., Wiley, New York, 1985, p. 902.
[33] M.B. Tarabrin, G.G. Shestakov, R.P. Evstigneeva, E.Yu. Bulychev, Pharm. Chem. J. 18 (1984) 572.
[34] S. Wang, W. Bonrath, H. Pauling, F. Kienzle, J. Supercrit. Fluids 17 (2000) 135.
[35] W. Bonrath, C. Dittel, L. Giraudi, T. Netscher, T. Pabst, Catal. Today 121 (2007) 65.
[36] M.C. Laufer, W. Bonrath, W.F. Hölderich, Catal. Lett. 100 (2005) 101.
[37] H. Wang, B.-Q. Xu, Appl. Catal. A Gen. 275 (2004) 247.